

COSMOLOGY WITH PHOTOMETRIC SURVEYS OF TYPE IA SUPERNOVAE

YAN GONG^{1,2,3}, ASANTHA COORAY¹, AND XUELEI CHEN^{2,4}

¹Department of Physics & Astronomy, University of California, Irvine, CA 92697

²National Astronomical Observatories, Chinese Academy of Sciences, Beijing, 100012, China

³Graduate School of Chinese Academy of Sciences, Beijing 100049, China and

⁴Center of High Energy Physics, Peking University, Beijing 100871, China

Draft version January 19, 2020

ABSTRACT

We discuss the extent to which photometric measurements alone can be used to identify Type Ia supernovae (SNIa) and to determine the redshift and other parameters of interest for cosmological studies. We fit the light curve data of the type expected from a survey such as the one planned with the Large Synoptic Survey Telescope (LSST) and also to remove the contamination from the core-collapse supernovae to SNIa samples. We generate 1000 SNIa mock flux data for each of the LSST filters based on existing design parameters, then use a Markov Chain Monte-Carlo (MCMC) analysis to fit for the redshift, apparent magnitude, stretch factor and the phase of the SNIa. We find that the model fitting works adequately well when the true SNe redshift is below 0.5, while at $z < 0.2$ the accuracy of the photometric data is almost comparable with spectroscopic measurements of the same sample. We discuss the contamination of Type Ib/c (SNIb/c) and Type II supernova (SNII) on the SNIa data set. We find it is easy to distinguish the SNII through the large χ^2 mismatch when fitting to photometric data with Ia light curves. This is not the case for SNIb/c. We implement a statistical method based on the Bayesian estimation in order to statistically reduce the contamination from SNIb/c for cosmological parameter measurements from the whole SNe sample. The proposed statistical method also evaluate the fraction of the SNIa in the total SNe data set, which provides a valuable guide to establish the degree of contamination.

Subject headings: cosmology: theory — distance scale — large-scale structure — supernovae: general

1. INTRODUCTION

The cosmological applications of luminosity-distance measurements to Type Ia supernovae (SNeIa) are now well known (Riess et al. 1998; Perlmutter et al. 1999; Leibundgut 2001). While the current sample of SNeIa-based distances are limited to a few hundred SNe (Astier et al. 2006; Wood-Vasey et al. 2007; Kowalski et al. 2008; Hicken et al. 2009; Kessler et al. 2009), future surveys are now planned to increase the sample size to a few thousand or more that could potentially allow a few percent accurate dark energy equation of state measurements in several redshift bins between $0 < z < 1$ (see e.g. Howell et al. 2009; Sarkar et al. 2008). The main challenge for constructing large samples are likely to be spectroscopic follow-up measurements to identify if each supernova detected in a photometric monitoring campaign is Type Ia and to establish the redshift of that supernova.

In addition to the planned space-based programs such as the Joint Dark Energy Mission (JDEM)¹, in the near future, there will also be several ground based photometric surveys for cosmological measurements and other astronomical studies. These include the Dark Energy Survey (DES)², the Pan-Starrs survey³, and ultimately the Large Synoptic Survey Telescope (LSST)⁴, which plans to monitor a large area of the sky every few days leading to a large sample of transient sources including supernovae. Given the large size of the samples of

SNe expected, it is highly unlikely to have spectroscopic follow-ups for all or even a large fraction of them. Due to this limitation it appears challenging to obtain cosmological measurements with the SNIa seen by LSST. Since LSST is likely to detect a few hundred thousand or more SNe per year, it would be highly desirable to identify whether a given SN as Type Ia or not, and to extract useful parameters such as redshift and luminosity with photometric data alone. If reliable techniques could be established, then even with a large degradation in accuracy for individual data compared with the case where spectroscopic data are also available, given the large number statistics expected, one could still aim to achieve a good measurement of cosmological parameters.

In this spirit we pursue a study to establish the extent to which photometric data from a survey like LSST can be used to identify SNeIa and to measure the cosmological parameters. We do this by fitting the photometric light curve data with sampling and errors consistent with LSST. Our mock SNe samples also include core-collapse supernovae and we vary the fractions expected based on the current rate estimates of various types of SNe. Our MCMC analysis are focused on a joint parameter estimation including the redshift, apparent magnitude, stretch factor and the phase of the SNIa. We find that the model fitting works adequately well when the true SNe redshift is below 0.5. At $z < 0.2$ photometric data of the type expected with LSST provide an accuracy vary close to the case when spectroscopic measurements are also available, with the redshift determined separately from photometric data leading to one less parameter in MCMC fits.

We also focus on the contamination of Type Ib/c (SNIb/c) and Type II supernova (SNII) on the SNIa data

¹ <http://jdem.gsfc.nasa.gov/>

² <http://www.darkenergysurvey.org/>

³ <http://pan-starrs.ifa.hawaii.edu>

⁴ <http://www.lsst.org/>

set. We find it is easy to distinguish the SNII from SNIa's through the large χ^2 mismatch in the fitting to Ia light curves. This is not the case for SNIb/c and they provide the main contamination to Ia measurements. In addition to a cut in χ^2 values, we implement a statistical Bayesian estimation method to reduce the contamination from SNIb/c in the subset of SNe sample selected for cosmological measurements. This technique also establishes statistically the fraction of the SNIa in the total SNe data set, which provides a valuable guide to the degree of contamination from Ib/c's.

We employ the filter functions as currently publicized by the LSST team in addition to survey parameters outlined in Ivezić et al. (2008). We note that while our work is focused towards a survey like LSST, others have also consider the use of photometric data alone for SNe distance measurements (Johnson & Crots 2006; Sullivan et al. 2006; Kuznetsova & Connolly 2007; Wang 2007; Kim & Miquel 2007; Zentner & Bhattacharya 2009).

The discussion is organized as follows. In the next Section we describe our procedure to simulate SNeIa data in a survey like LSST and move on to discuss our six parameter model fits to the multi-wavelength light curves from a large mock sample using a MCMC analysis. In Section 4, we discuss the contamination from Type II and Ib/c SNe to Ia photometric samples and a way to statistically reduce the contamination from Ib/c's using a technique that implements the Bayes theorem.

2. SIMULATING SNIA OBSERVED FLUX DATA

In this Section, we describe the process to generate the various SNe data. We first discuss the observed SNIa mock flux data.

2.1. The Mock Light Curve

The apparent observed flux from a supernova at z can be written as the convolution of the spectral energy distribution (SED) and the transmission function of the telescope,

$$f_{obs} = \int T_X(\lambda_{obs}) SED(\lambda_{obs}, t_{obs}, s, E_{B-V}^{host}, E_{B-V}^{MW}) d\lambda_{obs}, \quad (1)$$

where $T_X(\lambda_{obs})$ is the filter response for band X , λ_{obs} is the observed wavelength, t_{obs} is the observation date, s is the stretch factor, and E_{B-V}^{host} and E_{B-V}^{MW} are the color excess for the host galaxy and the Milky Way respectively.

The transmission functions used in our analysis for 5-bands of LSST are shown in Fig.1 (LSST filter draft 2005).⁵ We also plot rest-frame SEDs for Type Ia SNe at $z = 0.2, 0.5$, and 0.8 . These SED templates are from Nugent et al. (2002) and they cover the spectral wavelength from 1000 to 25000Å in rest-frame days from -20 to 70 with respect to the B-band maximum light day. The SNe flux for the epochs before -20 are set to be zero.

There are now several techniques to parameterize the SNIa light curves, such as the 15-day decline after the B-band maximum light Δm_{15} (Phillips 1993) and the

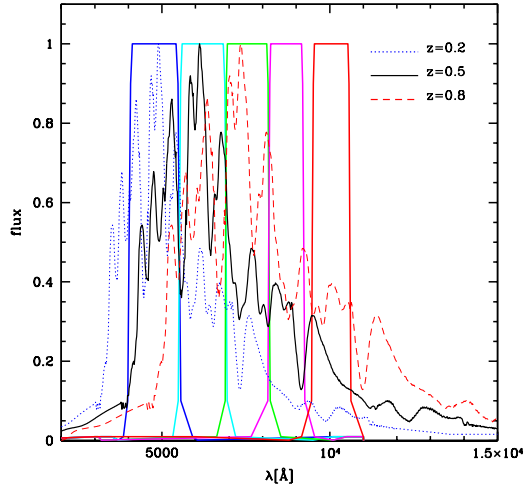


FIG. 1.— The LSST filters used in our analysis. From left to right are g, r, i, z and y-band functions. The Type Ia SEDs for SNe at $z = 0.2$, $z = 0.5$ and $z = 0.8$ are also shown. The flux is in an arbitrary unit.

multicolor light curve shape method (MLCS and the update version MLCS2k2) (Riess et al. 1996; Jha et al. 2007). In this paper, we calibrate the SNIa light curve with the time-scale and stretch factor relation following the works of Perlmutter et al. (1997, 1999). By stretching and compressing the time axis around the rest frame B-band maximum light day, this method can fit the observed light curve very well using the light curve template (Goldhaber et al. 2001). Then this SED can be re-scaled by the apparent, unextincted B-band peak magnitude

$$m_B = M_B + 5\log_{10}d_L(z, \theta) + 25 - \alpha(s - 1), \quad (2)$$

where M_B is the B-band absolute peak magnitude, d_L is the luminosity distance which is a function of the redshift z and a broad set of cosmological parameters denoted by θ and α is the coefficient of the relation between s and m_B . Here we take $M_B = -19.3$, $\alpha = 1.5$ (Knop et al. 2003; Astier et al. 2006), and the set of cosmological parameters θ with $\Omega_{m0} = 0.27$, $\Omega_{\Lambda0} = 0.73$ and $h_0 = 0.71$ (Komatsu et al. 2009) where Ω_{m0} and $\Omega_{\Lambda0}$ have the usual meaning with the present-day matter and dark energy density parameters and h_0 is the dimensionless Hubble constant. The B-band filter we use is from the Johnson-Morgan system (Bessell 1990, 2005). Also, the time scale of the SED is calibrated by the stretch factor s , which is assumed to be available from -15 to 35 around the B-band maximum luminosity day (Astier et al. 2006).

During the transit, the supernovae light will be partly absorbed by the dust of the host galaxy. We employ the reddening law of Cardelli et al. (1989) with $R_V = 3.1$, from infrared to far-ultraviolet ($0.3\mu m^{-1} \leq x \leq 10\mu m^{-1}$, where $x = 1/\lambda$). For the optical to near ultraviolet wavelength range ($1.1\mu m^{-1} \leq x \leq 3.3\mu m^{-1}$), we use an updated version for extinction given by O'Donnell (1994). The latter uses the same analytical form for extinction as Cardelli et al. (1989) but with values of the fitting parameters revised slightly from the previous version. The level of extinction we assume here is consistent with the one measured recently by Menard et al. (2009) corresponding to large angular scales based on galaxy-QSO cross-correlation in SDSS.

⁵ We note that there are several filter designs for LSST including a scenario involving 6 filters. Here, we focus on the 5-band case with simple filters.

Since the SNe are at a different redshift than the observer, the spectrum is redshifted for both wavelength and the phase, i.e. $\lambda' = \lambda(1+z)$ and $t' = t(1+z)$. We also apply an extinction associated with dust in the Milky Way (Burstein & Heiles 1982; Schlegel et al. 1998) with extinction applied randomly as described below. Finally, the spectrum is integrated with the LSST filters to get the mock light curve sampling in each of the 5 LSST filters.

Since the mean redshift of the SNe detections with LSST main survey is expected to be about 0.5, and the deeper, but smaller, survey can potentially detect SNe out to ~ 1 , we choose the redshift range from 0.01 to 1.1 when making mock SNe samples.

When creating large samples, the redshift z , stretch factor s and the extinction of the host galaxy E_{B-V}^{host} is generated from the Gaussian distribution as follow: $0.01 \leq z \leq 1.1$ with $\bar{z} = 0.5$ and $\sigma_z = 0.4$, $0.6 \leq s \leq 1.4$ with $\bar{s} = 1$ and $\sigma_s = 0.3$ and $-0.1 \leq E_{B-V}^{host} \leq 0.3$ with $\bar{E}_{B-V}^{host} = 0.0$ and $\sigma_E = 0.2$. Besides, we also consider the dispersion of the rest-frame B-band peak magnitude after the calibration of the stretch factor, Δm with $\bar{\Delta m} = 0.0$ and $\sigma_{\Delta m} = 0.17$. This extra dispersion acts as an extra source of noise in our mock data (Sullivan et al. 2006; Hamuy et al. 1995, 1996; Phillips et al. 1999; Guy et al. 2005).

2.2. The Photometric Error and The Cadence

The photometric error we use for LSST comes from Ivezić et al. (2008) and takes the form of

$$\sigma_{phot}^2 = \sigma_{sys}^2 + \sigma_{zero}^2 + \sigma_{rand}^2, \quad (3)$$

where σ_{sys} is the systematic photometric error which is designed to be very small ($< 0.005\text{mag}$), σ_{zero} is the absolute photometric error which we set to $\sigma_{zero} = 0.02\text{mag}$ (Astier et al. 2006; Sullivan et al. 2006), and σ_{rand}^2 is the random photometric error for point sources given by

$$\sigma_{rand}^2 = (0.04 - \gamma)x + \gamma x^2. \quad (4)$$

Here γ is a parameter related to the sky brightness and readout noise, among others. and $x = 10^{0.4(m-m_5)}$, where m is the magnitude and m_5 is 5σ depth for a detection of a point source in each of LSST bands. The m_5 is a function of the sky brightness, the seeing, the exposure time, atmospheric extinction, the airmass and the overall throughput of the instrument. All of the value of these parameter can be found in Table 2 of Ivezić et al. (2008).

We randomly generate the first observational day from -20 to 35 rest-frame days to ensure that we always have enough data to establish the stretch factor. We next randomly select the data point to occur every 3 or 4 days based on the cadence of the LSST (Ivezić et al. 2008). Finally, about 1000 mock SNIa flux data are generated for each of the five filters.

In Fig.2, we show the examples of the mock light curves in g, r and i bands at different redshifts. The mock flux is created from the Gaussian distribution with the mean on the light curve. Here we set the first observe-day $t_0^{obs} = -10$ in the observer-frame.

3. FITTING THE LIGHT CURVE

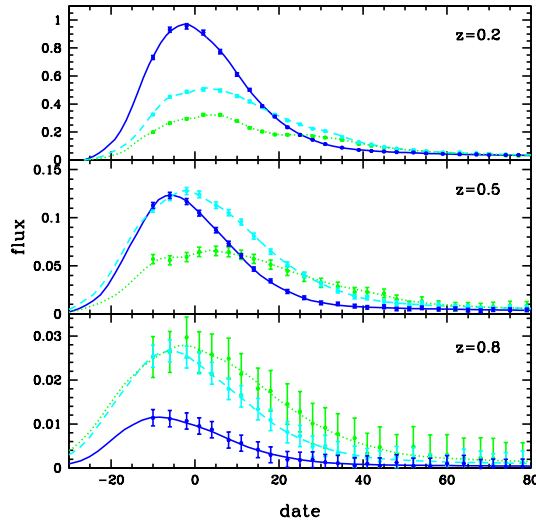


FIG. 2.— The examples of LSST mock SNIa light curves and observational data. The solid blue, dashed cyan and dotted green lines are the g, r and i band light curves respectively, and the first observe-day is set at -10 day in the observer-frame. The flux is in an arbitrary unit.

There are six light curve parameters that we hope to extract from multi-wavelength light curve fitting. These parameters are the z , m_B , s , E_{B-V}^{host} , Δm and t_0^{rest} (i.e. the rest-frame date for the first observe-day). The χ^2 statistical method is employed here with

$$\chi^2 = \sum_i^t \sum_j^{bands} \left\{ \frac{f_{ij}^{obs} - f_{ij}^{th}(T_j; z, t_i, s, E_{B-V}^{host}, E_{B-V}^{MW})}{\sigma_{ij}^{obs}} \right\}^2, \quad (5)$$

where f_{ij}^{obs} , σ_{ij}^{obs} and f_{ij}^{th} are the observed flux, error and theoretical flux for the observe-day t_i and band j , and T_j is the transmission of band j . The summation goes through all bands and days with observed samplings of the light curves.

3.1. The Markov Chain Monte Carlo Technique

Considering the number of the parameters, the efficiency and the accuracy, we employ the MCMC technique to perform the fitting process. This method does not require to assume a Gaussian distribution for the likelihood, and it is easy to perform the marginalization over other parameters when quoting error for one parameter. Most importantly, it is very efficient for the multi-parameter fitting (Neil 1993; Lewis & Bridle 2002; MacKay 2003; Doran & Mueller 2004; Gong & Chen 2007; Trotta 2008).

Our purpose is to estimate the posterior probability $P(\theta|\mathbf{D})$ for the parameter set θ given the observational data set \mathbf{D} . Based on the Bayes theorem

$$P(\theta|\mathbf{D}) = \frac{\mathcal{L}(\mathbf{D}|\theta)P(\theta)}{P(\mathbf{D})}, \quad (6)$$

where $\mathcal{L}(\mathbf{D}|\theta) \sim e^{-\chi^2/2}$ is the likelihood which denotes the probability to get \mathbf{D} given the parameters θ , $P(\theta)$ is the prior probability for θ and $P(\mathbf{D})$ is the normalization factor which would not affect our analysis here.

The Metropolis-Hastings algorithm is applied in our MCMC technique to decide if a new point should be ac-

cepted by an acceptance probability:

$$\mathbf{a}(\theta_{n+1}|\theta_n) = \min \left\{ \frac{P(\theta_{n+1}|\mathbf{D}) \mathbf{q}(\theta_n|\theta_{n+1})}{P(\theta_n|\mathbf{D}) \mathbf{q}(\theta_{n+1}|\theta_n)}, 1 \right\} \quad (7)$$

$$= \min \left\{ \frac{\mathcal{L}(\mathbf{D}|\theta_{n+1}) \mathbf{q}(\theta_n|\theta_{n+1})}{\mathcal{L}(\mathbf{D}|\theta_n) \mathbf{q}(\theta_{n+1}|\theta_n)}, 1 \right\}, \quad (8)$$

where $\mathbf{q}(\theta_{n+1}|\theta_n)$ is the proposal density to propose a new point θ_{n+1} given a current point θ_n in the chain. Here we assume uniform prior probabilities for the parameters which is canceled in Eq.(8). If $\mathbf{a} = 1$, the new point θ_{n+1} is accepted; otherwise, the new point is accepted with probability \mathbf{a} . This process are repeated until a new point is accepted, and then we set $\theta_n = \theta_{n+1}$. Also, we set a uniform Gaussian-distributed proposal density for every point, so that it is independent of the position on the chain, i.e. $\mathbf{q}(\theta_{n+1}|\theta_n) = \mathbf{q}(\theta_n|\theta_{n+1})$, we then have

$$\mathbf{a}(\theta_{n+1}|\theta_n) = \min \left\{ \frac{\mathcal{L}(\mathbf{D}|\theta_{n+1})}{\mathcal{L}(\mathbf{D}|\theta_n)}, 1 \right\}. \quad (9)$$

Since the proposal density determines the step size of the MCMC process, it is closely related to the convergence and mixing of the chain. Here we adopt the adaptive step size Gaussian sampler given by (Doran & Mueller 2004). The criterion of the convergence we use was described in Gelman & Rubin (1992), and after convergence we freeze the step size (Doran & Mueller 2004).

The ranges of the parameters are as follow: $z \in (0, 2)$, $m_B \in (10, 30)$, $s \in (0.5, 1.5)$, $E_{B-V}^{host} \in (-0.5, 0.5)$, $\Delta m \in (-0.3, 0.3)$ and $t_0^{rest} \in (-20, 40)$. For each mock SNIa, we take about 10000 chain points to illustrate the probability distribution of the parameters after the burn-in and thinning process.

3.2. The Light Curve Fitting Results

In Fig.3, we compare the input redshift of each of our 1000 SNIa in the simulation with the redshift obtained from MCMC fitting of SEDs to the multi-wavelength light curves. We find that when $z < 0.2$ the SNIa light curves are adequately sampled with enough accuracy to allow good redshift estimates along with other parameters, with uncertainties as small as 0.001. Such an error is comparable with the spectroscopic measurements, and even if the spectroscopic measurements could provide a higher precision on the measurement of the redshift, in any case the unknown bulk flows (Cooray & Caldwell 2006; Zhang & Chen 2008) would produce an error on the redshift at this level. For the medium redshift $0.2 < z < 0.5$, the estimated redshift is still useful but the uncertainty is about 0.1. For $z > 0.5$, the apparent magnitude becomes large, and since $\sigma_{phot} \sim 10^{0.4m}$, the redshift errors increase quickly with increasing redshift and can reach ~ 1 . The limitation at high redshift is also due to lack of near-IR photometric coverage and addition of IR bands beyond the z -band will improve photometric determinations when $z > 0.5$.

The residuals and 1σ errors for the total six fitting parameters in the MCMC analysis are shown in Fig.4. Similar to the redshift, the multi-wavelength light curve model fitting leads to parameter accuracies that are remarkably accurate when $z < 0.2$, except for Δm as it

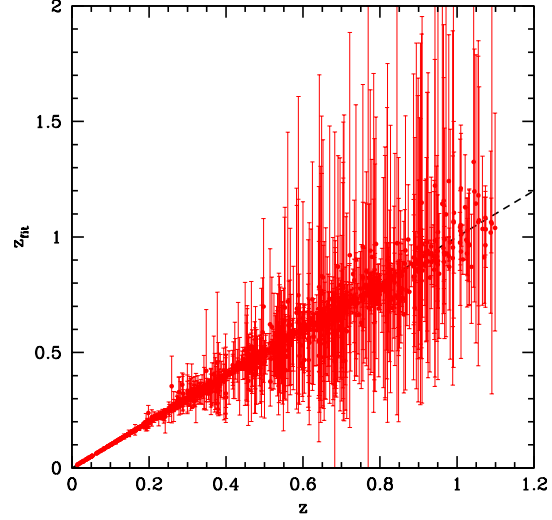


FIG. 3.— The intrinsic redshift of each of the 1000 mock SNIa light curves compared to the photometric redshift estimated with multi-parameter MCMC fits to multi-wavelength light curves. The best fit value and 1σ errors are shown. The redshift estimation is remarkably accurate at low redshifts when $z < 0.2$ with errors comparable to either the spectroscopic measurements of redshift or theoretical uncertainty in the redshift coming from peculiar velocities and bulk flows, among others. At $z > 0.5$, the fitted redshift errors are significantly larger because of the large photometric errors σ_{phot} .

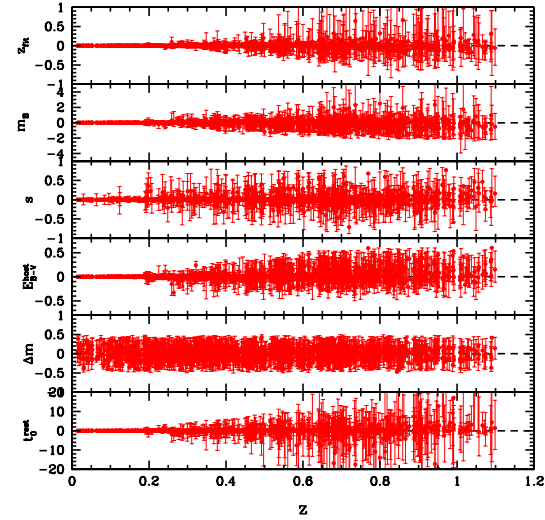


FIG. 4.— The residuals for the six parameters in the MCMC analysis with 1σ errors for the 1000 SNIa in the mock sample. The results are pretty good for $z < 0.2$, except for Δm since it can be seen as the noise and is independent on the redshift.

acts as an extra source of noise independent of the redshift. Over the whole redshift range studied out to z of 1.1, the dispersion of the fitting m_B , s , E_{B-V}^{host} and t_0^{rest} are mainly less than ± 1 , ± 0.3 , ± 0.4 and ± 4 , respectively.

3.3. The Constraints on Cosmology

To establish the overall effect of the uncertainty from photometric redshift for cosmological studies, we also generate 1000 SNIa with spectroscopic redshifts z_{spec} with the LSST photometric error σ_{phot} , i.e. we just fix the redshift and only model fit the other five parameters. The Hubble diagram for the spectroscopic and photomet-

ric cases are shown in Fig.5. Only one sixth of the whole data are shown on each figure.

We use the MCMC approach to fit the cosmological parameters from the two Hubble diagrams. Two cosmological scenarios are considered, that first one is Λ CDM with non-flat geometry and the second is w CDM with the time-evolved equation of state for the dark energy with $w(z) = w_0 + w_1 z / (1 + z)$.

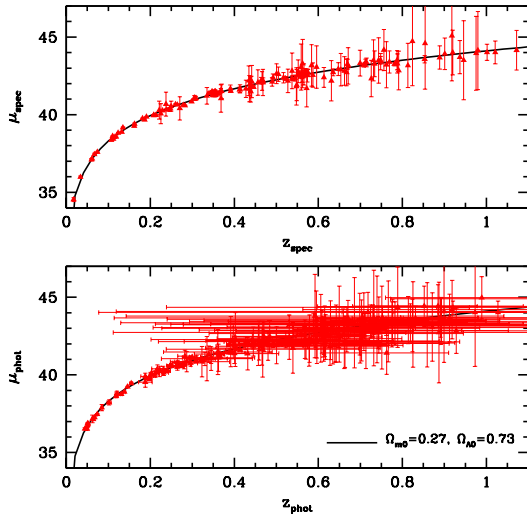


FIG. 5.— The Hubble diagram for the z_{spec} and z_{phot} simulations. The data points on each figure are just one sixth of the whole data sets.

In Fig.6, we show the contour maps of Ω_{m0} vs. $\Omega_{\Lambda 0}$ and w_0 vs. w_1 with 1σ and 2σ errors. As can be seen, the 1σ contours using z_{phot} and its error in cosmological parameter fits nearly overlap with the 2σ contours of the case where redshift is known precisely using z_{spec} . Also, we find little deviation for the directions of the main axis of the contours for the two cases. Thus, for a survey such as those planned for LSST, we effectively find a factor of ~ 2 degradation in parameter uncertainties when using the SNIa sample with only photometric redshifts compared with one with also spectroscopic redshifts. In terms of the dark energy figure of merit that involves the inverse area of the w_0 vs. w_1 ellipse, photometric SNe samples lead to a factor of 4 degradation compared to spectroscopic sample. This difference, however, is likely to be a minor issue: compared with the planned SNeIa surveys which will involve spectroscopic measurements of a few thousand SNe per year, photometric only surveys such as the one with LSST will produce a sample of a few hundred thousand SNe.

4. REMOVING THE CONTAMINATION FROM SNIb/c AND SNIi

In a pure photometric survey such as the one with LSST without spectroscopic measurements to identify if each of the SN is Type Ia or not, in addition to the error in the measurement of redshift, the photometric SNe samples would also be contaminated by core-collapse supernovae. Here we consider the contamination from Type Ib/c (SNIb/c) and Type II supernova (SNIi).

4.1. Estimating The Contamination

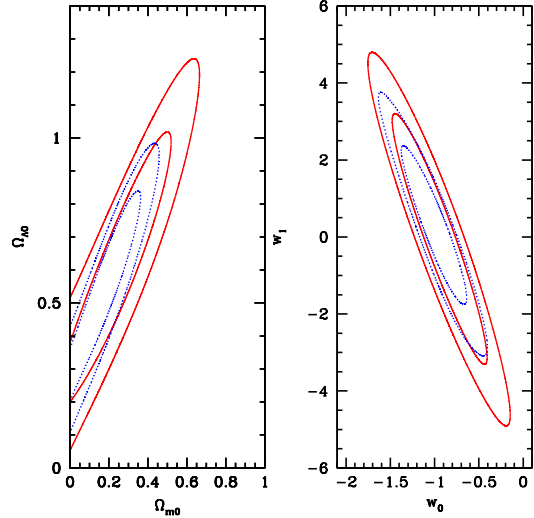


FIG. 6.— The contour maps for Ω_{m0} vs. $\Omega_{\Lambda 0}$ (left) and w_0 vs. w_1 (right). The 1σ and 2σ errors are shown. The red solid and blue dotted contours are for photometric and spectroscopic redshift simulations respectively.

To estimate the level of contamination, we create mock samples of light curve data for SNIb/c and SNIi. The spectral templates for SNIb/c is from Levan et al. (2005), and for SNIi we use the templates of SNIIP and SNIIL given by Gilliland et al. (1999) and Baron et al. (2004).⁶ Here, for simplicity, we consider primarily the SNIIP and SNIIL. The SNIi in which have “unusual” progenitors (Mobberley 2007) may be an important contamination for the SNIa (Poznanski et al. 2007b). We may discuss these objects in future work. We set the percentage of SNIIP and SNIIL are 50% and 50% respectively for the SNIi sample. The mock flux data of the SNIb/c and SNIi samples are generated with the same procedure as those used to generate the SNIa mock data in § 2.

Since the core-collapse supernovae are intrinsically fainter than the SNeIa and have no magnitude-phase relation, we take the absolute peak magnitude from Richardson et al. (2002) and the Gaussian distribution with $\bar{z} = 0.4$ for SNIb/c and SNIi, and then set $s = 1$ when mimicking their B-band peak magnitude. Also, given that the core-collapse supernovae are usually found in star forming regions, they are expected to suffer more extinction from the host galaxy. We set $-0.2 < E_{B-V}^{host} < 0.4$ with $\overline{E_{B-V}^{host}} = 0.0$ and $\sigma_E = 0.3$. Once simulated, we continue to use the SNIa SED light curves to fit them just as we did in § 3.

The distribution of relative χ^2 for the SNIa, SNIb/c and SNIi are shown in Fig.7. We find that when fitted with Ia SED light curves, the χ^2 values for SNeIi are so large large values that they are easily distinguished from the SNIa even with photometric data alone. However, for SNeIb/c the χ^2 peak overlaps with that of the SNeIa, so they are the primary contamination to the total sample.

To obtain a less-contaminated sample, as a first cut we note that the χ^2 distribution of the SNeIb/c has a long tail which can extend to tens of thousands, and some of the SNeIb/c can be removed by an overall restriction on the χ^2 values in the fitting to SNIa

⁶ http://supernova.lbl.gov/~nugent/nugent_templates.html

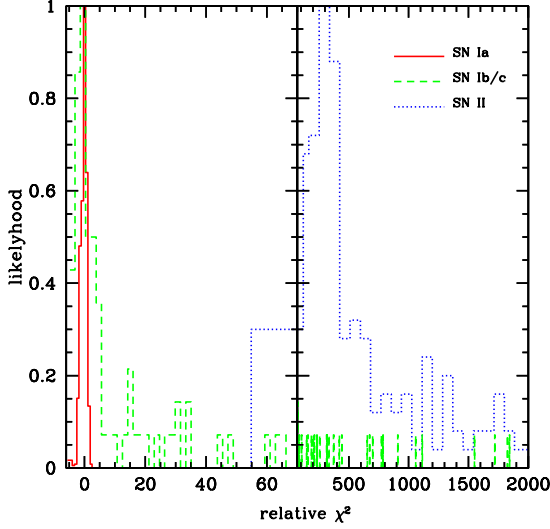


FIG. 7.— The distribution of relative χ^2 for the SNIa, SNIb/c and SNII samples when analyzed in all cases with Ia SED based light curves. The χ^2 distribution of SNII data are significantly than the same for SNIa. This allows Type II SNe that are contaminating Ia samples to be easily distinguished. However, the peak of the χ^2 distribution for the SNIb/c overlaps with the same for SNIa and we find SNIb/c to be the main contaminants for photometrically selected Ia samples for cosmological measurements.

light curve template. If the selection is restricted to $\chi_{rel}^2 < 20$, keeping all real Type Ia's, this results in a removal of about 40% of the SNIb/c's. Since the ratio of the rate of SNIa to SNIb/c out to $z \sim 1$ is about 10 to 7 (Calura & Matteucci 2006; de Plaa et al. 2007; Sato et al. 2007; Poznanski et al. 2007a; Eldridge et al. 2008; Smartt et al. 2009; Georgy et al. 2009), we expect about 250 SNIb/c to remain and contaminate a sample that contains 1000 SNIa selected photometrically. In the next subsection we discuss a statistical method to further reduce the contamination of Ib/c's during model fits to the total sample.

4.2. The Bayesian Statistical Method

We employ the Bayesian estimation method proposed by Press (1996) and Kunz et al. (2007) to further reduce the contamination from SNIb/c. We note that our proposed statistical method cannot distinguish each SNIb/c from a Type Ia individually, but statistically it reduces the overall contamination and the associated bias in cosmological parameters. As we illustrate here, the same method also allows us to jointly estimate the fraction of the SNIa (or Ib/c's) within the whole supernovae sample used for cosmology.

We take the case that the observational sample of supposedly Type Ia's \mathbf{D} contains a mixture of true SNIa data \mathbf{D}_1 and SNIb/c's \mathbf{D}_0 which mimicks Ia. We define a vector \mathbf{v} of length the total number of SNe N with the value of v_i taking either 1 or 0 if D_i is or is not a SNIa. We also define a quantity p to account for the total fraction of the true SNIa in the total SNe data set \mathbf{D} . Using \mathbf{v} and p , the posterior probability can be written as

$$P(\theta|\mathbf{D}) = \sum_{p, \mathbf{v}} P(\theta, \mathbf{v}, p|\mathbf{D}) \quad (10)$$

$$\propto \sum_{p, \mathbf{v}} \mathcal{L}(\mathbf{D}|\theta, \mathbf{v}, p) P(\theta, \mathbf{v}, p) \quad (11)$$

$$\propto \sum_{p, \mathbf{v}} \mathcal{L}(\mathbf{D}|\theta, \mathbf{v}, p) P(p) P(\theta|p) P(\mathbf{v}|\theta, p), \quad (12)$$

In Eq. (10), the sum over p will be the integration if the value of p is continuous, and the sum of \mathbf{v} goes through all 2^N possible values of \mathbf{v} . Eq. (11) is derived from the Bayes theorem, and $\mathcal{L}(\mathbf{D}|\theta, \mathbf{v}, p)$ is the likelihood. The $P(\theta|p)$ in Eq. (12) can be reduce to $P(\theta)$ since there is no reason to believe the parameter p affect the cosmological evolution of the Universe (it is not a cosmological parameter).

Thus, we can simplify to

$$P(\theta|\mathbf{D}) \propto P(\theta) \sum_p P(p) \sum_{\mathbf{v}} \mathcal{L}(\mathbf{D}|\theta, \mathbf{v}, p) P(\mathbf{v}|\theta, p). \quad (13)$$

Given p , $P(\mathbf{v}|\theta, p)$ is 0 when v_i involving the i th datum is a SNIb/c. When normalized, $P(v_i = 1|\theta, p) = p$ and $P(v_i = 0|\theta, p) = 1 - p$. Therefore, we find

$$P(\theta|\mathbf{D}) \propto P(\theta) \sum_p P(p) \sum_{\mathbf{v}} \left[\prod_{v_i=1} \mathcal{L}_i^1 p \prod_{v_i=0} \mathcal{L}_i^0 (1-p) \right]. \quad (14)$$

Here \mathcal{L}_i^1 is the likelihood that the i th SN is a Ia and this is taken to be

$$\mathcal{L}_i^1 = \frac{1}{\sqrt{2\pi}\sigma_i} e^{-\chi_i^2/2}, \quad (15)$$

where σ_i is the error and $\chi_i^2 = (\mu_i^{obs} - \mu_i^{th})^2/\sigma_i^2$, and the μ_i^{obs} and μ_i^{th} are the observational and theoretical distance modulus respectively.

The \mathcal{L}_i^0 is the likelihood for the SNIb/c samples though we don't know a priori the exact distribution. We use two parameters b and σ_0 belonging to the parameter set θ to describe P_i^0 as

$$\mathcal{L}_i^0 = \frac{1}{\sqrt{2\pi}\sigma_0} e^{-\chi_i^2/2}, \quad (16)$$

where $\chi_i^2 = (\mu_i^{obs} - \mu_i^{th} - b)^2/\sigma_0^2$.

We can simplify Eq.(14) further by noting that the 2^N summation term can be written as the product of N terms. We finally get

$$P(\theta|\mathbf{D}) \propto P(\theta) \sum_p P(p) \prod_N \left[\mathcal{L}_i^1 p + \mathcal{L}_i^0 (1-p) \right]. \quad (17)$$

The sum over p is easily performed with MCMC runs, and we assume $P(p)$ is a uniform distribution. When analyzing our mock samples we take the ranges for p , b and σ_0 of $p \in (0.5, 1)$, $b \in (-20, 20)$, $1/\sigma_0 \in (0, 1000)$.

4.3. The Results

Extending the discussion in §4.1, we add 250 SNIb/c data with $\chi_{rel}^2 < 20$ to the 1000 SNIa data, and extract cosmological constraints on the time-evolving equation of state of dark energy with an analysis which implements the Bayesian estimation method described above, in addition to a method where all data are analyzed with a MCMC run without making an attempt to account for Ib/c contamination to the total sample.

We show the contour maps of w_0 vs. w_1 in Fig.8. The red solid and blue dotted contours are the fitting results with and without Bayesian estimation, respectively. As can be seen in Fig.8, the constraint on w_0 and w_1 is completely wrong when we ignore the Ib/c contamination in

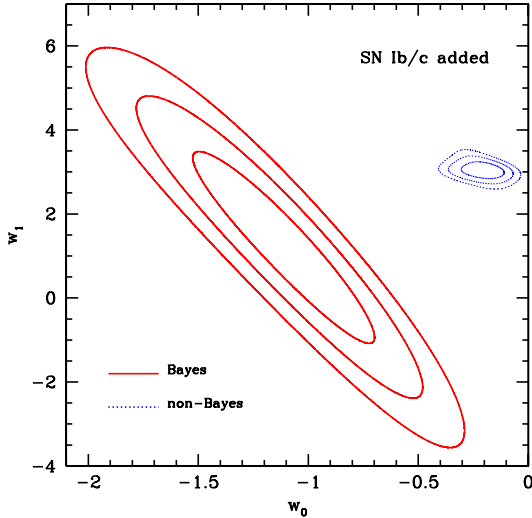


FIG. 8.— The contour maps for w_0 vs. w_1 with and without Bayesian estimation. The 1σ , 2σ and 3σ errors are shown.

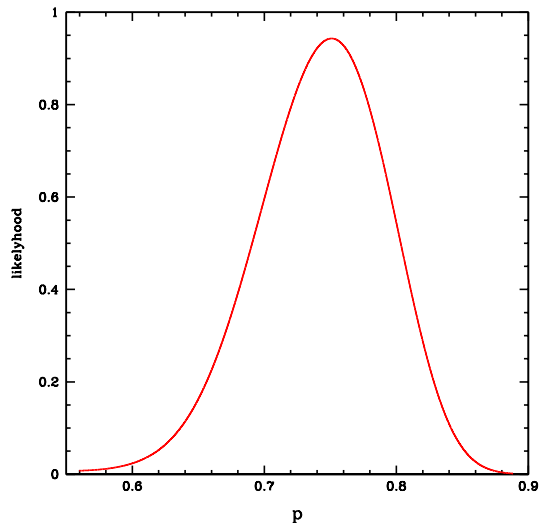


FIG. 9.— The PDF of the fraction p for the SNeIa in the mixed sample of Ia's and Ib/c's. The fiducial value is 0.8 while the fitting result based on the technique outlined in § 4.2 is $p = 0.75^{+0.05}_{-0.06}$.

the total sample and just do direct fitting to the Hubble diagram. This is caused by the large differences of the distribution between the SNIa and the SNIb/c data and MCMC chains are easily trapped in a wrong likelihood value. The χ^2 value for the overall best-fit in this case is also very large reaching as high as 2000.

When we implement the Bayesian estimation method, the result is improved significantly. Although there is a difference between the best fit and the actual (fiducial) value, the fiducial value of the cosmological parameter set $(w_0, w_1) = (-1, 0)$ lies safely within the 2σ contour around the best fit. Also, as discussed, we also jointly estimate the fraction of SNeIa in the total data set. We plot the likelihood for $P(p)$ in Fig.9. The fraction of the SNIa in this particular mock data should be 80% while the fitting leads to the result of $p = 0.75^{+0.05}_{-0.06}$ with errors at 1σ . While there still remains a bias associated with the contaminating Type Ib/c's, we have reduced this bias

to the level of a few percent.

We believe the Bayesian estimation method provides a useful statistical tool to reduce contamination and to evaluate the fraction of the contaminating supernovae in the LSST photometric SNIa survey. Of course, to identify whether each individual SN is a core-collapse one or a Ia, the method discussed above is inadequate, but the Bayesian statistical analysis can be a valuable guide for further advanced study (Poznanski et al. 2002; Gal-Yam et al. 2004; Johnson & Crots 2006; Poznanski et al. 2007b; Kuznetsova & Connolly 2007).

5. SUMMARY

In this paper, we explore the ability to determine the redshift and the other parameters useful to construct the Hubble diagram with light curve for the LSST SNIa photometric measurements. Using a SNIa SED template and the expected photometric error of the LSST, we first simulate the observed flux data of 1000 SNIa in each of 5 LSST filters, and then apply a MCMC technique to fit the redshift, stretch factor, apparent magnitude and the phase of the SNIa, among others. We find that when $z < 0.2$, these parameters can be determined accurately at a level comparable to the case where spectroscopic redshift is known. At higher redshifts, the uncertainty in photometric redshift goes up quickly since $\sigma_{phot} \sim 10^{0.4m}$, but the photometric data is still very useful when $0.2 < z < 0.5$. To illustrate the effect of the uncertainty of the photometric redshift on the fitting of the cosmological parameters, we also extract cosmological constraints using parameters of the SNIa light curves with and without spectroscopic redshifts. Using the fitting results of the two cases, we constrain the cosmological parameters for Ω_{m0} and $\Omega_{\Lambda 0}$ in the Λ CDM model and w_0 and w_1 in the time-evolved wCDM model. We find that for the same number of SNIa data, the cosmology fitting with only the photometric data leads to a factor of 2 degradation in error of cosmological parameters or a factor of 4 in the figure of merit of dark energy equation of state (i.e. the inverse area of the $w_0 - w_1$ ellipse) compared with the case of fitting with spectroscopic data. However, as the number of photometric-only data far exceeds that with spectroscopic data, the overall statistical uncertainty in the former would still be smaller.

Finally, we discuss the contamination on the SNIa data from core-collapse supernovae involving types II and Ib/c, and the feasibility of using a Bayesian estimation statistical method to reduce the overall contamination. Similar to SNIa mock samples, we generate the mock flux data for the SNIb/c and SNII based on their spectral templates, and use the SNIa fitting process to fit them. We find that the SNeII are easily distinguished from SNIa because there is an apparent mismatch (large χ^2) when fitting with the SNIa templates. However, this is not the case for Type Ib/c's. The peak of its χ^2 distribution is overlapping with that of the SNIa and present a significant contamination of any photometric selected supposedly SNIa samples, even if a conservative cut is applied in the χ^2 values for selection. To further account for this contamination, at least statistically when doing cosmological model fits, we employ Bayes theorem. Our suggested method could reduce the contamination down to a few percent level, leading to estimates of cosmological parameters that are biased within 1σ errors. The

method also establishes the fraction true SNIa in the total photometric SNe data set. Nevertheless, we must note that this method cannot distinguish if an individual SN is whether Type Ia or not. We will need an extended analysis complemented with additional observations if we are required to recognize the type of individual SNe.

This research is supported by the NSF under CAREER AST-0645427 at UCI, by the NSFC under the Distin-

guished Young Scholar Grant 10525314, the Key Project Grant 10533010, by the Chinese Academy of Sciences under grant KJCX3-SYW-N2, and by the Ministry of Science and Technology of China under the National Basic Science program (project 973) grant 2007CB815401. X.C. also acknowledges the hospitality of the Moore Center of Theoretical Cosmology and Physics at Caltech, where part of this research is performed.

REFERENCES

- Astier, P., et al. 2006, *A&A*, 447, 31
 Baron, E., et al. 2004, *ApJ*, 616, 91
 Bessel, M., S. 1990, *Publ.Astron.Soc.Pac.*, 102, 1181
 Bessell, M., S. 2005, *Annu. Rev. Astron. Astrophys.*, 43, 293
 Burstein, D. & Heiles C. 1982, *AJ*, 87, 1165B
 Calura, F. & Matteucci, F. 2006, *ApJ*, 652, 889
 Cardelli, J., A., Clayton, G., C. & Mathis, J., S. 1989, *ApJ*, 345, 245
 Cooray, A. & Caldwell, R. R., 2006, *Phys. Rev. D*, 73, 103002
 de Plaa, J. et al. 2007, *A&A*, 465, 345
 Doran, M. & Mueller, C., M. 2004, *JCAP* 0409 003
 Eldridge, J., J., Izzard, R., G. & Tout, C., A. 2008, *Massive Stars as Cosmic Engines*, Proceedings of the International Astronomical Union, IAU Symposium, 250, 179
 Gal-Yam, A. et al. 2004, *PASP*, 116, 597
 Gelman, A. & Rubin, D. 1992, *Statist.Sci.*, 7, 457
 Georgy, C. et al. 2009, *arXiv:0906.2284*
 Gilliland, R. L., Nugent, P. E., & Phillips, M. M. 1999, *ApJ*, 521, 30
 Goldhaber, G., et al. 2001, *ApJ*, 558, 359
 Gong, Y. & Chen, X. 2007, *Phys. Rev. D*, 76, 123007
 Guy, J., Astier, P., Nobili, S., Regnault, N., & Pain, R. 2005, *A&A*, 443, 781
 Hamuy, M., Phillips, M. M., Maza, J., Suntzeff, N. B., Schommer, R. A., & Aviles, R. 1995, *AJ*, 109, 1
 Hamuy, M., Phillips, M. M., Suntzeff, N. B., Schommer, R. A., Maza, J., & Aviles, R. 1996, *AJ*, 112, 2391
 Hicken, M. et al., 2009, *ApJ*, 700, 1097
 Howell, D.A. et al., "Type Ia supernova science 2010-2020", white paper submitted to Astro2010, *arXiv:0903.1086*.
 Ivezić, Z., et al., 2008, *arXiv:0805.2366*
 Jha, S., Riess, A., G. & Kirshner, R., P. 2007, *ApJ*, 659, 122
 Johnson, B., D., & Crotts, A., P., S. 2006, *AJ*, 132, 756
 Kessler, R. et al., 2009, *arXiv:0908.4274*.
 Kim, A. & Miquel, R. 2007, *Astropart.Phys.*, 28, 448
 Knop, R. A., et al. 2003, *ApJ*, 598, 102
 Komatsu, E., et al. 2009, *ApJS*, 180, 330
 Kowalski, M. et al., 2008, *ApJ*, 686, 749.
 Kunz, M., Bassett, B., A. & Hlozek, R. 2007, *Phys. Rev. D*, 75, 103508
 Kuznetsova, N., V. & Connolly, B., M. 2007, *ApJ* 659 530
 Leibundgut, B., 2001, *ARA&A*, 39, 67.
 Levan, A., et al. 2005, *ApJ*, 624, 880
 Lewis, A. & Bridle, S. 2002, *Phys. Rev. D*, 66, 103511
 LSST Filter Design Document-DRAFT 3-8-05 (2005); available at http://www.wiyn.org/ODI/LSST_Filter_Doc.3.8.05.pdf
 MacKay, D., J., C. 2003, *Information Theory, Inference and Learning Algorithms*
 Menard, B., Scranton, R., Fukugita, M. & Richards, G. 2009, *arXiv:0902.4240*
 Mobberly, M. 2007, *Supernovae and How to Observe Them*
 Neil, R., M. 1993, *Probabilistic Inference Using Markov Chain Monte Carlo Methods*
 Nugent, P., Kim, A. & Perlmutter, S. 2002, *Publ.Astron.Soc.Pac.*, 114, 803
 O'Donnell, J., E. 1994, *ApJ*, 422, 158
 Perlmutter, S., et al. 1997, *ApJ*, 483, 565
 Perlmutter, S., et al. 1999, *ApJ*, 517, 565
 Phillips, M. M. 1993, *ApJ*, 413, L105
 Phillips, M. M., Lira, P., Suntzeff, N. B., Schommer, R. A., Hamuy, M., & Maza, J. 1999, *AJ*, 118, 1766
 Poznanski, D., et al. 2002, *PASP*, 114, 833
 Poznanski, D., Maoz, D. & Gal-Yam, A. 2007, *AJ*, 134, 1285
 Poznanski, D., et al. 2007, *MNRAS*, 382, 1169
 Press, W., H. 1996, *Unsolved Problems in Astrophysics*
 Richardson, D., et al. 2002, *AJ*, 123, 745
 Riess, A. G., Press, W. H., & Kirshner, R. P. 1996, *ApJ*, 473, 88
 Riess, A. G. et al., 1998, *AJ*, 116, 1009
 Sarkar, D. et al. 2008, *PRL*, 100, 241302
 Sato, K. et al. 2007, *ApJ*, 667, L41
 Schlegel, D. J., Finkbeiner, D., P. & Davis, M. 1998, *ApJ*, 500, 525
 Smartt, S., J., Eldridge, J., J., Crockett, R., M. & Maund, J., R. 2009, *MNRAS*, 395, 1409
 Sullivan, M., et al. 2006, *AJ*, 131, 960
 Trotta, R. 2008, *Contemporary Physics*, 49, 71
 Wang, Y. 2007, *ApJ*, 654, L123CL125
 Wood-Vasey et al., 2007, *ApJ*, 666, 694.
 Zentner, A. & Bhattacharya, S., 2009, *ApJ*, 693, 1543
 Zhang, P. & Chen, X., 2008, *Phys. Rev. D*, 78, 023006